

000 BEYOND TEXT-TO-IMAGE: LIBERATING GENERATION 001 WITH A UNIFIED DISCRETE DIFFUSION MODEL 002

003 **Anonymous authors**
004

005 Paper under double-blind review
006

007 ABSTRACT 008

009 Unified generation models aim to handle diverse tasks across modalities—such
010 as text-to-image generation and image-to-text generation—within a single archi-
011 tecture and decoding paradigm. Autoregressive unified models suffer from slow
012 inference due to sequential decoding, and non-autoregressive unified models suf-
013 ffer from weak generalization due to limited pretrained backbones. We introduce
014 Mudit, a **unified discrete diffusion** transformer that enables fast and parallel
015 generation across both text and image modalities. Unlike prior unified diffusion
016 models trained from scratch, Mudit integrates strong **visual priors** from a pre-
017 trained text-to-image backbone with a lightweight text decoder, enabling flexible
018 and high-quality multimodal generation under a unified architecture. Empirical
019 results show that Mudit achieves competitive or superior performance compared
020 to significantly larger autoregressive models in both quality and efficiency. The
021 work highlights the potential of purely discrete diffusion, when equipped with
022 strong visual priors, as a scalable and effective backbone for unified generation.
023

024 1 INTRODUCTION 025

026 Unified generative models have recently emerged as a promising paradigm for multimodal data, en-
027 compassing both text and images. Most existing approaches adopt the autoregressive (AR) frame-
028 work (Touvron et al., 2023), where modalities are represented as discrete token sequences and gen-
029 erated sequentially in raster order. While this paradigm is well-suited for language, it introduces
030 severe inefficiencies in image generation: producing an image requires step-by-step prediction of
031 thousands of tokens, leading to substantial computational cost. Moreover, the imposed rasterized
032 order is poorly aligned with the inherently two-dimensional structure of images. These limita-
033 tions hinder speed/quality trade-offs and restrict flexible conditional generation, such as inpainting,
034 thereby constraining the practical applicability of unified models in interactive or real-time scenar-
035 os. To mitigate these issues, recent works (Chen et al., 2025a; Pan et al., 2025; Chen et al., 2025b)
036 have proposed hybrid approaches that couple AR-based language models with diffusion-based im-
037 age generators (Ho et al., 2020), as shown in Fig. 1 (a). However, such “glue” architectures fall short
038 of true unification, as they introduce additional complexity into the inference pipeline while retain-
039 ing considerable computational overhead. So there is a lack of a principled multimodal generative
040 paradigm over current unified models.
041

042 As shown in Fig 1 (b), recent work like Dual-Diffusion (Li et al., 2024c) explores unifying multi-
043 modal under the diffusion model, but it ultimately relies on continuous diffusion for image (Esser
044 et al., 2024) and discrete diffusion for text (Swerdlow et al., 2025b). This fundamental mismatch
045 in generative principles undermines its claim of a true unification paradigm. UniDisc (Swerdlow
046 et al., 2025a) takes a more promising step by applying discrete diffusion over multimodal token
047 spaces¹. This allows parallel refinement of text and image tokens, improving inference efficiency
048 and enabling more flexible conditioning. However, the overall quality of UniDisc’s generation re-
049 mains far from satisfactory. For example, it fails to match the fidelity of early diffusion models such

050 ¹MaskGIT, MaskAR, RandomAR, and Discrete Diffusion share significant conceptual and practical over-
051 laps, often differing only in decoding order or architectural nuances. We elaborate on their connections in the
052 next section. While Meissonic (Bai et al., 2025) follows the naming convention of MaskGIT (Chang et al.,
053 2022), we standardize terminology in this paper by referring to all such models under the umbrella of Discrete
054 Diffusion.

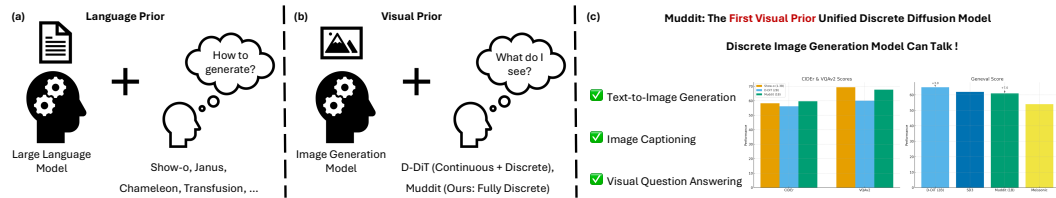


Figure 1: We propose **Muddit**, the first unified discrete diffusion model with a visual prior. Compared to language prior models like Show-o (Xie et al., 2024), Muddit demonstrates strong performance at image captioning and visual question answering. It also delivers clearer gains (7.0 vs 3.0) in image generation over the visual prior model D-DiT (Li et al., 2024c).

as Stable Diffusion 1.5 (Rombach et al., 2022), and lacks support for vision-language reasoning tasks such as visual question answering (VQA). We attribute these shortcomings to the pretrained model’s lack of prior knowledge. Without modular components carrying rich priors, these models face generalization and scalability bottlenecks.

Taken together, the two dark clouds: ineffective unified paradigm and the lack of strong prior knowledge, highlight the need for a new generation of unified models. In this work, we present **Muddit**, a MaskGIT-style unified discrete diffusion transformer equipped with a lightweight text decoder. By combining the strengths of parallel discrete diffusion and semantically rich visual priors from a pretrained Meissonic text-to-image backbone (Bai et al., 2025), Muddit enables scalable, efficient, and flexible sampling while significantly improving alignment and quality across modalities and various tasks such as high-resolution text-to-image generation, image captioning, and visual question answering, as shown in Fig. 1 (c).

We systematically detail the training objective of unified discrete diffusion models, the masking strategy, and the shared inference sampling strategy across three tasks. Finally, we conduct comprehensive evaluations with current popular unified models on several benchmarks, including GenEval, CIDEr, VQAv2, GQA, MME, MMBench, and MMMU, demonstrating Muddit’s superior performance and efficiency, validating that the unexplored purely discrete diffusion approach can rival, or even surpass, much larger autoregressive-based unified models. While concurrent unified generation models (Yang et al., 2025b) often build upon a language modeling prior—leveraging pretrained dLLMs as the backbone—we instead take a visual-first approach. Muddit is built upon an image generation prior, offering a new path toward unifying vision and language tasks within a discrete diffusion framework. We hope that this work inspires a new trend for unified generative modeling, grounded in discrete diffusion, beyond the boundaries of traditional text-to-image generation (Bai et al., 2025).

2 METHOD

2.1 DISCRETE DIFFUSION WITH UNIFIED IMAGE AND TEXT PERSPECTIVE

In discrete diffusion, a sample $x \in \mathcal{X}$ is treated as a one-hot vector \mathbf{x} , where $\mathcal{X} = \{1, \dots, N\}$. For language models, N equals the vocabulary size. While for image models, N is the number of discrete image token IDs obtained from a tokenizer or VQ codebook. At each diffusion step, we stochastically corrupt the tokens, gradually transforming the data distribution into a maximally entropic categorical prior; the generative model then learns to invert this corruption. Following recent works (Lou et al., 2023; Bai et al., 2025) that cast token corruption as a continuous-time Markov chain (CTMC) over the finite alphabet \mathcal{X} , we let

$$\frac{dp_t}{dt} = Q_t p_t, \quad (1)$$

where $p_t \in \mathbb{R}^{N+1}$ is the distribution of x_t , the time-dependent matrix Q_t transports the data distribution $p_0 \approx p_{\text{data}}$ to the maximally entropic “noise” distribution $p_1 = p_{\text{stationary}}$. We adopt the absorbing-state (masked) diffusion variant that has proved particularly effective in text modelling: every symbol can jump to a dedicated mask token $\mathbf{m} = (\underbrace{0, \dots, 0}_N, 1)$ but never leaves it, i.e. \mathbf{m} is an absorbing class.

108 **Forward posterior.** Marginalising \mathbf{x} gives
 109

$$110 \quad q(x_t | \mathbf{x}) = \text{Cat}(x_t | \alpha_t \mathbf{x} + (1 - \alpha_t) \mathbf{m}). \quad (2)$$

111 $\text{Cat}(\cdot)$ denotes a categorical distribution; it returns a one-hot token sampled from the probability
 112 vector inside the parentheses. $\alpha_t \in [0, 1]$ is the *survival probability*, *i.e.* the probability that an
 113 individual token has not yet been masked by time t . Thus x_t equals the original clean token with
 114 probability α_t and equals the mask token \mathbf{m} with probability $1 - \alpha_t$.

115 **Reverse process.** For any $0 < s < t < 1$, the CTMC induces an analytic posterior
 116

$$117 \quad q(x_s | x_t, \mathbf{x}) = \begin{cases} \text{Cat}(x_s | x_t), & x_t \neq \mathbf{m}, \\ 118 \quad \text{Cat}(x_s | \frac{(1 - \alpha_s)\mathbf{m} + (\alpha_s - \alpha_t)\mathbf{x}}{1 - \alpha_t}), & x_t = \mathbf{m}, \end{cases} \quad (3)$$

120 x_t and x_s are the corrupted tokens at times t and s ($s < t$). If x_t is already a real vocabulary token
 121 ($x_t \neq \mathbf{m}$) it stays unchanged going backwards; otherwise, when $x_t = \mathbf{m}$, the distribution over x_s
 122 is a convex combination of the mask and the clean token \mathbf{x} , weighted by their respective survival
 123 probabilities α_s and α_t .

124 **Training Objective.** We employ a masked-token predictor $x_\theta(x_t, \alpha_t) \approx \mathbf{x}$, which leads to the
 125 continuous-time negative ELBO
 126

$$127 \quad \mathcal{L}_{\text{NELBO}} = \mathbb{E}_{q(x_t | \mathbf{x})} \left[\int_0^1 \frac{\alpha'_t}{1 - \alpha_t} \log(x_\theta(x_t, \alpha_t) \cdot \mathbf{x}) dt \right], \quad (4)$$

128 where $\alpha'_t = \frac{d\alpha_t}{dt}$ and \mathbf{x} is the one-hot vector of ground truth. $x_\theta(x_t, \alpha_t) \in \mathbb{R}^{N+1}$ is the model's
 129 predicted categorical probability vector for the clean token given the corrupted input (x_t, α_t) ; \mathbf{x} is
 130 the one-hot ground-truth clean token.

131 During generation, we start from an all-mask sequence ($t = 1$) and integrate the reverse CTMC
 132 towards $t = 0$, repeatedly replacing every masked position with the model's categorical prediction.
 133 Because the corruption schedule and objective are *identical* for any discrete alphabet \mathcal{X} , the same
 134 diffusion backbone unifies text and image generation. In the following section, we present Mudit,
 135 a unified framework that leverages discrete diffusion to model the generation tasks for both text and
 136 image jointly.

137 2.2 MUDDIT

138 2.2.1 UNIFIED ARCHITECTURE

139 As shown in Fig. 2, our architecture comprises a text encoder E_{txt} , image encoder E_{img} , transformer
 140 generator G , sampler S , text decoder D_{txt} , and image decoder D_{img} . The generator G is a single
 141 MM-DiT model, following the dual-/single-stream design of FLUX (Labs, 2024). Importantly,
 142 the generator G is initialized from the Meissonic (Bai et al., 2025), which has been extensively
 143 trained for high-resolution text-to-image generation. This initialization brings in a strong pretrained
 144 image prior, capturing rich spatial structures and semantic correlations across image and text tokens,
 145 which significantly enhances sample quality and accelerates convergence in the multimodal setting.
 146 Consequently, the same MM-DiT predicts the masked tokens for both modalities, which produces a
 147 shared generator for text and image synthesis.

148 To reduce the computational cost of high-resolution imagery and lengthy captions, we quantize both
 149 modalities into a compact discrete space. A pre-trained VQ-VAE acts as the image encoder E_{img} ,
 150 mapping pixels to codebook indices, while the CLIP text model, as E_{txt} , provides the text token
 151 embeddings. The MM-DiT predicts clean tokens in this shared space, which a lightweight linear
 152 head D_{txt} converts back to text tokens.

153 2.2.2 UNIFIED TRAINING

154 **Masking strategy.** We model the forward posterior in Eq. 2 of both modalities using time-dependent
 155 hyperparameters α_t , with the mask ratio defined as $\gamma_t = 1 - \alpha_t$. While BERT (Devlin, 2018)
 156 employs a fixed mask ratio of 15%, this setting is suitable for token completion but insufficient for
 157 generation. To support generative tasks, the design of γ_t must satisfy the following criteria:

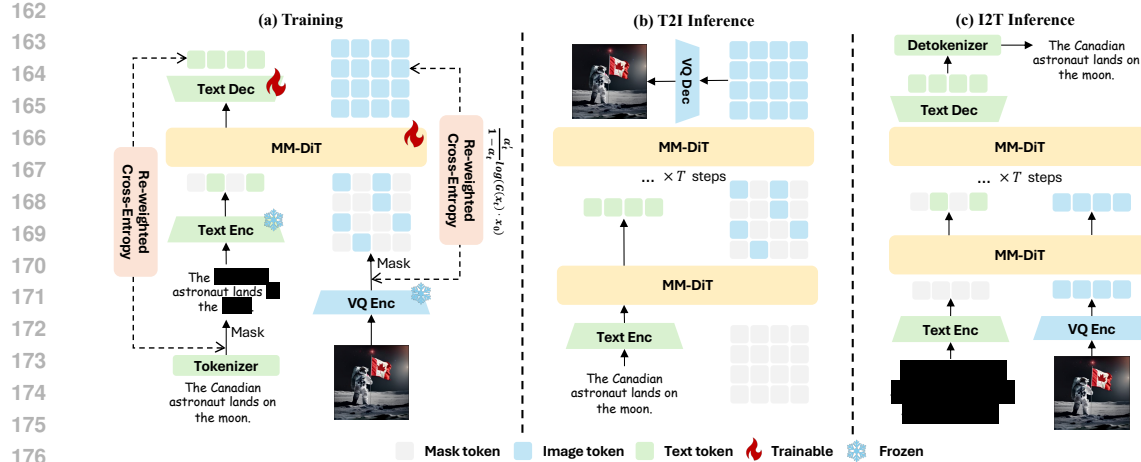


Figure 2: The training and inference architecture of Mudit. **(a)** During training, we randomly mask tokens from one of the two modalities. MM-DiT is trained to predict the masked tokens using a re-weighted cross-entropy loss, which jointly optimizes both the MM-DiT backbone and a lightweight text decoder. **(b)** In text-to-image inference, we initialize the image latent features using all-masked tokens and iteratively predict each latent token via MM-DiT. **(c)** In image-to-text inference, we similarly initialize all text tokens as masked and generate the text through the same iterative decoding process. Specifically for VQA tasks, we append mask token IDs to the end of the question and predict all masked token IDs as the final answer.

1. γ_t must be a continuous function, bounded between 0 and 1, for $t \in [0, 1]$.
2. γ_t should monotonically decrease with respect to t , with boundary conditions $\gamma_0 \rightarrow 0$ (initially clean data) and $\gamma_1 \rightarrow 1$ (masking all tokens).

Several strategies for masking and sampling have been proposed to meet these criteria (Chang et al., 2022). We adopt *cosine scheduling strategy*. During training, a timestep $t \in [0, 1]$ is sampled from a truncated arccos distribution, with the density function:

$$\gamma_t = \frac{2}{\pi}(1 - (1 - t)^2)^{-\frac{1}{2}}. \quad (5)$$

During training, a mask ratio $\gamma_t \in [0, 1]$ is randomly sampled for each modality \mathbf{x}_0 (either image or text tokens), and the forward process (Eq. 2) is applied by randomly replacing clean tokens with mask tokens to obtain \mathbf{x}_t .

Unified training objective. Let \mathbf{c} denote the conditioning: the text embedding when synthesizing an image, or the image embedding when generating a caption. We randomly sample a mask ratio by Eq. 5. Then we corrupt the target sequence \mathbf{x}_0 (image or text tokens) with the CTMC described in Eq. 1 and train a single masked-token predictor $\mathbf{G}(\mathbf{x}_t, \alpha_t, \mathbf{c})$ to reconstruct \mathbf{x}_0 . Both directions—text \rightarrow image and image \rightarrow text—share the identical continuous-time negative ELBO

$$\mathcal{L}_{\text{unified}} = \mathbb{E}_{q(\mathbf{x}_t | \mathbf{x})} \left[\int_0^1 \frac{\alpha'_t}{1 - \alpha_t} \log(\mathbf{G}(\mathbf{x}_t, \alpha_t, \mathbf{c}) \cdot \mathbf{x}) dt \right], \quad (6)$$

where all symbols are as in Eq. 4 but the \mathbf{G} now receives the cross-modal condition \mathbf{c} as an additional input. **Key point:** switching from text \rightarrow image to image \rightarrow text merely changes the conditioning signal \mathbf{c} ; the loss Eq. 6 itself is unchanged. This symmetry keeps optimization identical across tasks and allows us to train a single parameter set jointly for both generation directions. During inference we again start from an all-mask sequence ($t=1$) and integrate the reverse CTMC towards $t=0$, feeding in the desired condition \mathbf{c} to obtain either an image or a sentence from the same diffusion backbone.

216 2.2.3 UNIFIED INFERENCE
217218 **Sampling strategy.** During inference, we apply the time-reversed posterior as defined in Eq. 3.
219

220
$$S(G, x_t, t) = p_\theta(x_s | x_t) = \begin{cases} \text{Cat}(x_s | x_t), & x_t \neq \mathbf{m}, \\ \text{Cat}\left(x_s | \frac{(1 - \alpha_s)\mathbf{m} + (\alpha_s - \alpha_t)G(x_t, \alpha_t, \mathbf{c})}{1 - \alpha_t}\right), & x_t = \mathbf{m}, \end{cases} \quad (7)$$

221
222
223

224 where θ denotes the parameters of G , \mathbf{c} is the multimodal condition, and α_t in Eq. 5 is applied
225 sequentially with t taking values $1, \frac{T-1}{T}, \dots, \frac{1}{T}$, where T is the total number of reverse steps. At
226 each timestep t , Muddit predicts a fraction $\gamma_{t+\frac{1}{T}} - \gamma_t$ of the masked tokens by G and update the
227 masked tokens x_t by S , continuing iteratively until all masked tokens are recovered. This dynamic
228 approach offers several advantages over autoregressive methods, which require the model to learn
229 conditional probabilities $P(x_i | x_{<i})$ based on a fixed token ordering. In contrast, random masking
230 with a variable ratio enables the model to learn $P(x_i | x_\Lambda)$, where Λ denotes an arbitrary subset of
231 observed tokens. This flexibility is essential for parallel sampling, allowing multiple tokens to be
232 predicted simultaneously rather than sequentially.
233233 Our Muddit supports three tasks with a single generator G and sampler S : (i) text \rightarrow image, (ii) image
234 \rightarrow text (captioning), and (iii) visual–question answering (VQA). The only change across tasks is the
235 conditioning source \mathbf{c} provided to G ; the diffusion process and guidance logic are shared.
236236 **(i) Text \rightarrow image.** Given a text prompt $tp \in \mathcal{T}$, the text encoder E_{txt} produces a text token embedding
237 $c_{\text{txt}} = E_{\text{txt}}(tp)$. Starting from a fully masked sequence x_1 , the generator produces logits
238

239
$$l_t = G(x_t, \alpha_t, c_{\text{txt}}), \quad x_{t-\frac{1}{T}} = S(l_t, x_t, t), \quad (8)$$

240

240 for $k = 1, \frac{T-1}{T}, \dots, \frac{1}{T}$. After T steps we obtain visual tokens x_0 , which the image decoder D_{img}
241 converts to a pixel-space image $I = D_{\text{img}}(x_0)$.
242243 **(ii) Image \rightarrow text.** For captioning, an input image $I \in \mathcal{I}$ is tokenized by the image encoder E_{img} :
244 $c_{\text{img}} = E_{\text{img}}(I)$. The generator now conditions on the *visual* tokens while progressively decoding
245 text:
246

247
$$l_t = G(x_t, \alpha_t, c_{\text{img}}), \quad x_{t-\frac{1}{T}} = S(l_t, x_t, t), \quad (9)$$

248

248 yielding a text token sequence x_0 , which D_{txt} maps to a caption $\text{caption} = \text{Detokenize}(D_{\text{txt}}(x_0))$.
249250 **(iii) Image + question \rightarrow answer (VQA).** For visual–question answering we supply *both* an image
251 and a question: $c_{\text{img}} = E_{\text{img}}(I)$ and $c_{\text{txt}} = E_{\text{txt}}(q)$. They are concatenated and fed to the generator,
252 which outputs logits over answer tokens x_k :
253

254
$$l_t = G(x_t, \alpha_t, [c_{\text{img}}, c_{\text{txt}}]), \quad x_{t-\frac{1}{T}} = S(l_t, x_t, t), \quad (10)$$

255

255 until the full answer a is produced and decoded by $a = \text{Detokenize}(D_{\text{txt}}(x_0))$.
256257 **Classifier-free guidance.** At each decoding step, we apply the same guidance rule, independent of
258 modality:
259

259
$$l_k \leftarrow G(z_k, \alpha_k, \mathbf{c}) + \lambda[G(z_k, \alpha_k, \mathbf{c}) - G(z_k, \alpha_k, \mathbf{c}_{\text{neg}})], \quad (11)$$

260

260 where z_k (image or text tokens) is the partial target sequence, \mathbf{c} is the *positive* condition (prompt,
261 image, or image +question), \mathbf{c}_{neg} is the corresponding negative condition, and λ is the guidance scale.
262 Because the loss, decoding schedule, and guidance operator are *identical* in all three scenarios—only
263 the conditioning signal changes—our framework realises a genuinely unified multimodal generator.
264265 3 EXPERIMENT
266267 3.1 EXPERIMENTAL SETUP
268269 **Implementation details.** We build Muddit on top of the open-sourced Meissson models (Bai et al.,
270 2025). The MM-DiT backbone is initialized with pretrained weights, and a lightweight linear head

is added as a text decoder. Following Meissonic, we adopt the CLIP (Radford et al., 2021) as text encoder and VQ-VAE as image encoder and decoder, keeping them entirely frozen throughout all experiments. To support discrete denoising, we append a special `<mask>` token to CLIP’s vocabulary for text masking, while the image mask token is inherited directly from Meissonic’s initialization. We observe that, even without training, the `<mask>` embedding can already be predicted into a coherent sentence during training. Therefore, for simplicity, we freeze the `<mask>` embedding. During training, we use a constant learning rate of 1×10^{-4} and a weight decay of 1×10^{-2} . Gradient accumulation is applied in both pretraining and supervised fine-tuning, resulting in an effective batch size of 1024. We trained on 16 H100 GPUs for 5 days. During inference, we adopt the default Meissonic configuration, using cosine masking scheduling, 64 sampling steps, and a classifier-free guidance (CFG) scale of 9.0 and 1.5 for text-to-image and image-to-text generation, respectively.

Training data. We train Muddit in two stages using a combination of publicly available and internal datasets, including JourneyDB (Pan et al., 2023), LAION-Art (Schuhmann et al., 2022), CC12M (Changpinyo et al., 2021), and others. The final dataset is filtered based on aesthetic score, resolution, and aspect ratio, resulting in approximately 10 million image–text pairs. Both stages are optimized with the unified training objective defined in Eq. 6. Below, we describe the datasets and settings for each stage in detail.

- 1. Pretraining.** We pretrain Muddit for 100K steps with a batch size of 1024, using the unified objective across both modalities. Text inputs are truncated to a maximum of 77 tokens, and images are resized to 512×512 . The pretraining corpus consists of 8 million image–text pairs, re-captioned using Qwen2.5-VL-3B for improved consistency. Each batch is evenly split between text-to-image and image-to-text samples to enable joint training in both directions.
- 2. Instruction tuning.** After pretraining, we fine-tune the model on a combination of 1 million instruction following datasets, including LLaVA-Instruct-150K, ALLaVA, SA-1B, and the VQAv2 training set. During this stage, only the answer portion of each prompt is masked. Additionally, we construct a curated dataset of 1 million high quality image–text pairs to support multi-task training on VQA and image generation. Following the task instructions embedded in each sample, Muddit learns to produce long-form answers, concise replies, and image captions via task-specific prompting.

We present both quantitative and qualitative results for the T2I and I2T tasks in the following sections. Additional experiments and ablation studies are provided in the Appendix.

3.2 TEXT-TO-IMAGE GENERATION

Quantitative results. Following prior work, we evaluate our 512×512 model on GenEval (Ghosh et al., 2024) after supervised fine-tuning. Muddit attains an overall accuracy of 0.61, surpassing prior discrete diffusion models such as Monetico (0.44) and Meissonic (0.54), and closely matching Stable Diffusion 3 (0.62) with only 1B parameters. It further shows strong compositional reasoning (0.72 on “Two Objects”, 0.54 on “Counting”), and benefits from joint multimodal training, which enhances T2I performance. These results demonstrate the effectiveness of Muddit as the first unified discrete diffusion model for both text and image modalities.

Qualitative results. We present diverse generations from our model conditioned on rich textual prompts in Fig. 3. The outputs exhibit strong text-image alignment, capturing fine details in both realistic and imaginative scenes. Our model effectively renders complex structures, lighting, and textures across various domains.

3.3 IMAGE-TO-TEXT GENERATION

We present a comprehensive comparison of our model Muddit against other multimodal models across four benchmarks: MS-COCO (image captioning) (Lin et al., 2014), VQAv2 (Antol et al., 2015), MME (Fu et al., 2023), MMBench (Liu et al., 2024e), GQA (Hudson & Manning, 2019), and MMMU (Yue et al., 2024) in Tab. 2. Notably, Muddit is the first unified model to employ discrete diffusion for both text-to-image and image-to-text generation, demonstrating that this approach is not only viable but also highly competitive.

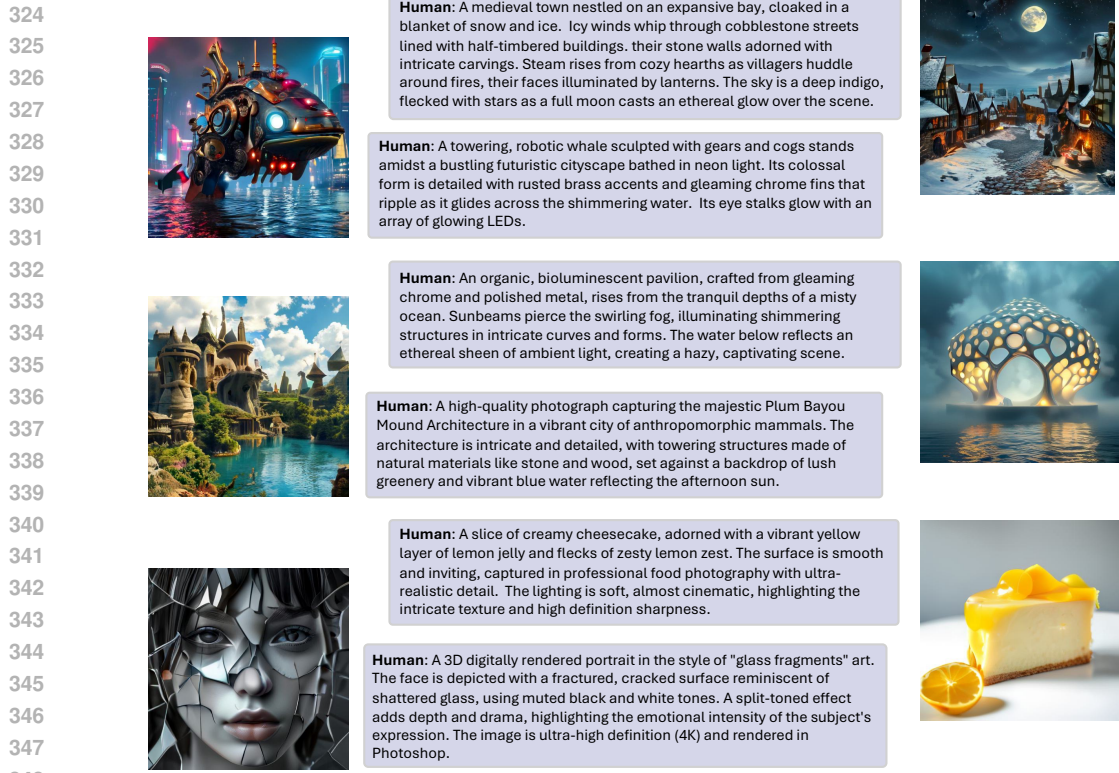


Figure 3: Samples of Text-to-Image Generation by Mudit.

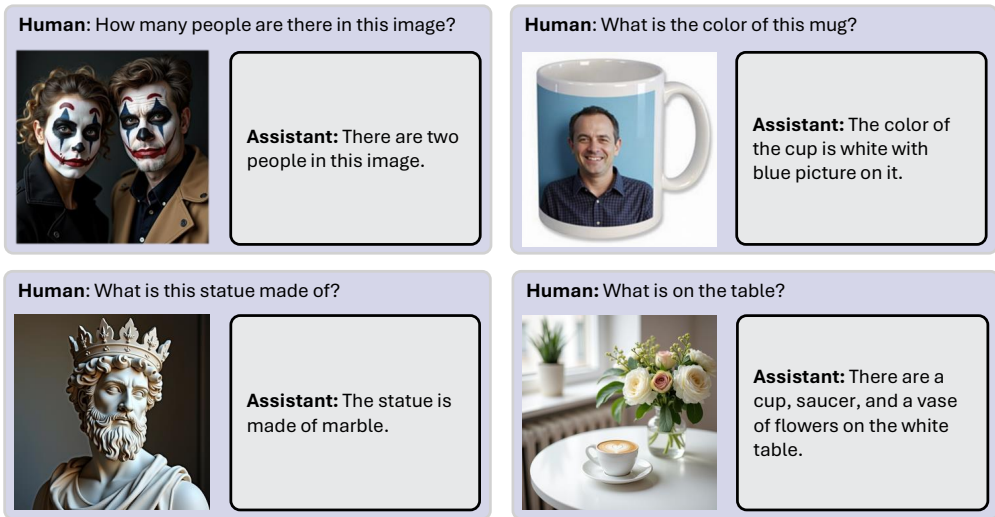


Figure 4: Samples of Visual Question Answering by Mudit.

369
370
371
372
373
374
375
376
377

Quantitative comparison. Mudit demonstrates strong performance across benchmarks despite its compact size (1B parameters). It achieves a CIDEr score of 59.7 on MS-COCO, surpassing diffusion-based baselines such as D-DiT (56.2) and Show-O (46.8–65.5). On VQAv2, it attains 67.7% accuracy, outperforming Show-O and D-DiT while approaching larger autoregressive models like LLaVA-Next (82.8%). Moreover, it reaches 1104.6 on MME, 28.4 on MMB, and 57.1 on GQA, underscoring its competitiveness across multimodal reasoning tasks. These results highlight the effectiveness of Mudit as a unified diffusion-based model that balances efficiency with high-quality task performance.

Qualitative results. We present example captions generated by our model across diverse scenarios in Fig. 5, including humans, animals, vehicles, and natural landscapes. The model demonstrates

378 Table 1: Evaluation of text-to-image generation performance on the GenEval (Ghosh et al., 2024).
379

380 Model	Text Gen Arch	Image Gen Arch	Params (B)	Overall ↑	Objects ↑ Single Two	Counting ↑	Colors ↑	Position ↑	Color ↑ Attribution
381 PixArt- α (Chen et al., 2024b)	-	Diffusion	0.6	0.48	0.98 0.50	0.44	0.80	0.08	0.07
382 SD 2.1 (Rombach et al., 2022)	-	Diffusion	0.9	0.50	0.98 0.51	0.44	0.85	0.07	0.17
383 DALL-E 2 (Ramesh et al., 2022)	-	Diffusion	6.5	0.52	0.94 0.66	0.49	0.77	0.10	0.19
384 SDXL (Podell et al., 2023)	-	Diffusion	2.6	0.55	0.98 0.74	0.39	0.85	0.15	0.23
385 DALL-E 3 (Betker et al., 2023)	-	Diffusion	-	0.67	0.96 0.87	0.47	0.83	0.43	0.45
386 SD 3 (Esser et al., 2024)	-	Diffusion	2	0.62	0.98 0.74	0.63	0.67	0.34	0.36
387 LWM (Liu et al., 2024c)	AR	AR	7	0.47	0.93 0.41	0.46	0.79	0.09	0.15
388 SEED-X (Ge et al., 2024)	AR	AR	17	0.49	0.97 0.58	0.26	0.80	0.19	0.14
389 Chameleon (Team, 2024)	AR	AR	7	0.39	-	-	-	-	-
390 Show-O (Xie et al., 2024)	AR	Discrete Diff.	1.3	0.68	0.98 0.80	0.66	0.84	0.31	0.50
391 Transfusion (Zhou et al., 2024)	AR	Diffusion	8	0.67	-	-	-	-	-
392 D-DiT (Li et al., 2024b)	Discrete Diff.	Diffusion	2	0.65	0.97 0.80	0.54	0.76	0.32	0.50
393 Monetico (512 × 512) (Bai et al., 2025)	-	Discrete Diff.	1	0.44	0.92 0.48	0.26	0.78	0.06	0.13
394 Meissonic (1024 × 1024) (Bai et al., 2025)	-	Discrete Diff.	1	0.54	0.99 0.66	0.42	0.86	0.10	0.22
395 UniDisc (512 × 512) (Swerdlow et al., 2025b)	Discrete Diff.	Discrete Diff.	1.4	0.42	0.92 0.47	0.15	0.67	0.13	0.19
396 Muddit (512 × 512)	Discrete Diff.	Discrete Diff.	1	0.61	0.98 0.72	0.54	0.82	0.19	0.41



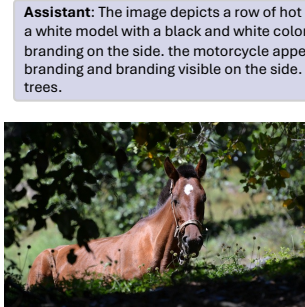
Assistant: The image depicts a man standing in water, holding a black dog and smiling. The man is wearing a yellow and wet jacket, and he has a happy expression. The background consists of a calm body of water with possibly a lake.



Assistant: The image depicts two individuals standing in a lush, forested area. the person on the left is older and wearing a light blue shirt and dark pants, while the person on the right is dressed in a suit with a shirt and tie. both appear to be engaged in a discussion or discussing something on the documents, with the person on the left holding a tablet.



Assistant: The image depicts a group of sheep walking along a road near a body of water, possibly a lake or a body of water water, possibly a sea or sea. the road is lined with small rocks and a scattered vegetation, and a road is visible on the side of the road. in the background, there are rolling hills and a calm water with a fence.



Assistant: The image depicts a row of hot motorcycles parked in a parking lot. the motorcycle is a white model with a black and white color scheme, identifiable by its distinctive design and branding on the side. the motorcycle appears to be a modern model model, as evidenced by the branding and branding visible on the side. the background includes a residential building, some trees.



Assistant: The image depicts a brown horse standing amidst a lush, green forest. the horse appears to be a thoroughbred horse, characterized by its dense features and tail visible. it is equipped with a bridle and a decorative tag on its forehead. the background is filled with dense foliage and small plants, suggesting a natural, foreforested environment. the overall scene is serene.

419 Figure 5: Samples of Image-to-Text Generation by Mudit.
420

421 strong visual grounding and fine-grained descriptive ability, accurately capturing attributes such as
422 clothing, expressions, background context, and object relationships. Fig. 4 illustrates our model’s
423 ability to accurately answer visual questions across various domains, including object counting,
424 color recognition, material identification, and compositional reasoning.

426 3.4 ABLATION STUDY AND ANALYSIS
427

428 **Analysis of the inference timesteps.** As shown in Tab. 5, performance generally improves with
429 more diffusion steps, plateauing around $T = 32$. GenEval and CIDEr see large gains from $T = 8$
430 to $T = 32$, with diminishing returns afterward. VQAv2 remains stable across timesteps, indicating
431 that fewer steps suffice for discriminative tasks. Overall, a moderate number of steps provides a
good balance between accuracy and efficiency.

432 Table 2: Evaluation of image captioning, visual question answering on multimodal benchmarks.
433

Model	Params (B)	Text Gen Arch	Image Gen Arch	MS-COCO CIDEr \uparrow	VQAv2 Acc. \uparrow	MME Acc. \uparrow	MMB Acc.	GQA Acc. \uparrow	MMMU Acc.
InternVL-2.0	8	AR	-	-	-	1648.1	81.7	61.0	49.3
LLaVA-Next	13	AR	-	-	82.8	1575.0	70.0	65.4	36.2
BLIP-2	13	AR	-	-	65.0	1293.8	-	41.0	34.4
Qwen-VL	7	AR	-	-	78.2	1487.5	-	57.5	35.9
OpenFlamingo	9	AR	-	65.5	43.5	-	-	-	28.7
Flamingo	9	AR	-	79.4	51.8	-	-	-	-
Chameleon	7	AR	AR	18.0	-	-	19.8	-	-
LWM	7	AR	AR	-	55.8	-	-	-	-
Show-O (256×256)	1.3	AR	Discrete Diff.	-	64.7	1014.9	-	54.2	-
Show-O (512×512)	1.3	AR	Discrete Diff.	-	69.4	1097.2	-	58.0	27.4
Transfusion	7	AR	Diffusion	29.0	-	-	-	-	-
D-DiT (256×256)	2	Discrete Diff.	Diffusion	-	59.5	897.5	-	55.1	-
D-DiT (512×512)	2	Discrete Diff.	Diffusion	56.2	60.1	1124.7	-	59.2	-
UniDisc	1.4	Discrete Diff.	Discrete Diff.	46.8	-	-	-	-	-
Muddit (512×512)	1	Discrete Diff.	Discrete Diff.	59.9	68.2	1107.4	28.4	57.5	27.6

434 Table 3: Impact of text loss weight. We apply
435 the same text loss weight during both pretrain-
436 ing and instruction tuning.

Benchmark	0.2	0.4	0.6	0.8	1.0
GenEval	60.1	60.5	61.6	60.8	58.3
MS-COCO	51.4	52.1	59.9	58.8	59.4
VQAv2	62.7	66.2	68.2	68.4	69.2

437 **Analysis of the text loss weight.** As shown in
438 Tab. 3, moderate text loss weights (around 0.6)
439 yield the best overall performance. CIDEr and
440 GenEval peak near this value, suggesting that
441 both insufficient and excessive text weighting can
442 harm generation quality. VQAv2 continues to im-
443 prove with stronger text supervision but begins to
444 plateau beyond 0.6. Overall, while discriminative
445 tasks benefit from heavier textual guidance,
446 generative tasks require a balanced mix of visual
447 and textual signals—highlighting the importance
448 of grounding language in multimodal learning.

449 **Analysis of joint training.** Joint optimization over both text-to-image (T2I) and image-to-text
450 (I2T) objectives is essential. As shown in Tab. 4, joint training yields the highest GenEval score,
451 outperforming both T2I-only and I2T-only variants. Notably, I2T-only causes GenEval to drop
452 sharply from 61.6 to 28.3—more than a twofold decrease—while MS-COCO CIDEr remains nearly
453 unchanged and VQAv2 declines only slightly. These results show that separating the objectives
454 severely weakens cross-modal integration, underscoring the need for unified optimization to main-
455 tain strong multimodal coherence.

456 3.5 THE SCALABILITY OF MUDDIT

457 To demonstrate the scalability of our approach, we curate roughly 10 million image–text pairs from
458 LIAON-ART (Schuhmann et al., 2022), JourneyDB (Pan et al., 2023), and CC12M (Changpinyo
459 et al., 2021). We filter out samples with an aesthetic score below 7, a height or width under 512
460 pixels, or an aspect ratio above 2. All images are re-captioned using Qwen2.5-VL 7B (Bai et al.,
461 2023). We pretrain Muddit on this dataset with a batch size of 512 and a resolution of 1024, applying
462 random masking to both image and text modalities. The image and text loss weights are set to 1.0
463 and 0.3, respectively. Training runs for 100K steps.

464 For instruction tuning, we collect about 6M samples from LLaVA-Instruct-150K (Liu et al., 2024d),
465 ALLAUA LAION (Chen et al., 2024a), SA-1B (Kirillov et al., 2023), ART500K (Mao et al., 2017),
466 ScienceQA (Lu et al., 2022), Chart2Text (Kantharaj et al., 2022), and VQAv2 (Antol et al., 2015).
467 Muddit is then trained with a batch size of 512 at a resolution of 1024, with masking applied only to
468 the answer text. We also add a 2M high-quality image dataset for high-quality fine-tuning. Further
469 training configurations are provided in Tab. 6. All experiments are conducted on 16 H100 GPUs.

470 We evaluate the scaled Muddit model against other comparably sized unified models and state-of-
471 the-art unified discrete diffusion models (Xin et al., 2025; Yang et al., 2025a), as shown in Tab. 7.

472 Table 4: Effect of joint training. We denote
473 text-to-image as T2I and image-to-text as I2T,
474 respectively.

Benchmark	T2I only	I2T only	Joint training
GenEval	59.3	28.3	61.6
MS-COCO	-	60.1	59.9
VQAv2	-	69.1	68.2

475 Table 5: Performance across different diffusion
476 timesteps.

Sample steps	GenEval	CIDEr	VQAv2
T=8	51.6	43.6	53.9
T=16	58.5	59.3	57.4
T=24	59.3	59.4	62.3
T=32	61.9	59.7	65.4
T=40	61.7	60.1	66.8
T=64	61.1	59.9	68.2

486
487
488 Table 6: Training hyperparameters across different training stages.
489
490
491
492
493
494
495
496

Hyperparameters	Stage-I (Pre-training)	Stage-II (Instruction-tuning)
Learning Rate	1.0×10^{-4}	1.0×10^{-4}
LR Scheduler	Constant	Constant
Weight Decay	0.01	0.01
Max Gradient Norm	10.0	10.0
Optimizer	AdamW ($\beta_1 = 0.9$, $\beta_2 = 0.999$)	
Batch Size	512	512
Training Steps	100K	15K
Training GPUs	16×H100	16×H100
Gen. Resolution	1024	1024
Under. Resolution	1024	1024

497
498
499
500 Table 7: Quantitative comparison with other unified models.
501
502
503
504
505
506

Model	Params	Base model	Architecture	Data scale	Geneval w TTS	VQAv2	MME	MMMU
Lumina-DiMOO	8B	LLaDA	Discrete Diff.	80M	0.92	–	1534.2	58.6
MMaDA (512×512)	8B	LLaDA	Discrete Diff.	Unknown	0.66	76.7	1410.7	30.2
Show-O (512×512)	1.3B	Phi-1.5	AR + Discrete Diff	35M	–	69.4	1097.2	27.4
D-DiT (512×512)	2B	SD3-medium	Discrete Diff + Diff	40M	–	60.1	1124.7	–
Mudit (512×512)	1B	Meismonic	Discrete Diff	10M	0.64	68.2	1107.4	27.6
Mudit (1024×1024)	1B	Meismonic	Discrete Diff	16M	0.67	70.2	1139.2	28.7

507
508 Across established benchmarks, Mudit exhibits consistent improvements in both image generation
509 and image understanding, empirically validating the scalability of our model. Furthermore, we com-
510 pare Mudit with unified models of similar parameter sizes, all of which rely on hybrid architectures.
511 Despite being trained on substantially less data, Mudit achieves superior performance.
512

513 We attribute this data efficiency to two key factors. First, our visual prior naturally maintains strong
514 text-following capability for text-to-image generation, enabling robust alignment between image
515 and text modalities. From the perspective of unified modeling, we prioritize cross-modal alignment
516 over isolated single-modality ability, which allows Mudit to reach higher performance with less
517 training data. Second, Mudit adopts a fully unified modeling paradigm: the model learns by pre-
518 dicting mask tokens based on context across all tasks (text-to-image and image-to-text). In contrast,
519 hybrid architectures must simultaneously handle next-token prediction alongside velocity or mask
520 prediction, and often introduce additional special tokens (e.g., `< soi >`, `< eoi >`), which increases
521 architectural complexity and hinders optimization.

4 CONCLUSION

523 In this work, we present Mudit, a unified generative framework that employs discrete diffusion to
524 bridge text and image modalities. By unifying image and text generation within a single model,
525 Mudit demonstrates strong performance across text-to-image, image-to-text, and VQA tasks. Notably,
526 it outperforms or matches the capabilities of significantly larger autoregressive models, while
527 enabling fast, parallel inference. Our results validate the effectiveness of discrete denoising as a
528 general-purpose modeling strategy and highlight its potential to serve as a scalable backbone for
529 future multimodal systems.

530
531
532
533
534
535
536
537
538
539

540 REFERENCES

542 Stanislaw Antol, Aishwarya Agrawal, Jiasen Lu, Margaret Mitchell, Dhruv Batra, C Lawrence Zit-
 543 nick, and Devi Parikh. Vqa: Visual question answering. In *Proceedings of the IEEE international*
 544 *conference on computer vision*, pp. 2425–2433, 2015.

545 Jinbin Bai, Tian Ye, Wei Chow, Enxin Song, Qing-Guo Chen, Xiangtai Li, Zhen Dong, Lei Zhu,
 546 and Shuicheng Yan. Meissono: Revitalizing masked generative transformers for efficient high-
 547 resolution text-to-image synthesis. *ICLR*, 2025.

548 Jinze Bai, Shuai Bai, Shusheng Yang, Shijie Wang, Sinan Tan, Peng Wang, Junyang Lin, Chang
 549 Zhou, and Jingren Zhou. Qwen-vl: A versatile vision-language model for understanding, local-
 550 ization, text reading, and beyond, 2023. URL <https://arxiv.org/abs/2308.12966>.

551 Hangbo Bao, Li Dong, Songhao Piao, and Furu Wei. Beit: Bert pre-training of image transformers.
 552 *arXiv preprint arXiv:2106.08254*, 2021.

553 James Betker, Gabriel Goh, Li Jing, Tim Brooks, Jianfeng Wang, Linjie Li, Long Ouyang, Juntang
 554 Zhuang, Joyce Lee, Yufei Guo, et al. Improving image generation with better captions. *Computer*
 555 *Science.*, 2:3, 2023.

556 Huiwen Chang, Han Zhang, Lu Jiang, Ce Liu, and William T Freeman. Maskgit: Masked generative
 557 image transformer. In *Proceedings of the IEEE/CVF Conference on Computer Vision and Pattern*
 558 *Recognition (CVPR)*, pp. 11315–11325, 2022.

559 Soravit Changpinyo, Piyush Sharma, Nan Ding, and Radu Soricut. Conceptual 12M: Pushing web-
 560 scale image-text pre-training to recognize long-tail visual concepts. In *CVPR*, 2021.

561 Guiming Hardy Chen, Shunian Chen, Ruifei Zhang, Junying Chen, Xiangbo Wu, Zhiyi Zhang, Zhi-
 562 hong Chen, Jianquan Li, Xiang Wan, and Benyou Wang. Allava: Harnessing gpt4v-synthesized
 563 data for a lite vision-language model, 2024a.

564 Juhai Chen, Zhiyang Xu, Xichen Pan, Yushi Hu, Can Qin, Tom Goldstein, Lifu Huang, Tianyi
 565 Zhou, Saining Xie, Silvio Savarese, Le Xue, Caiming Xiong, and Ran Xu. Blip3-o: A family of
 566 fully open unified multimodal models-architecture, training and dataset, 2025a. URL <https://arxiv.org/abs/2505.09568>.

567 Junsong Chen, Jincheng Yu, Chongjian Ge, Lewei Yao, Enze Xie, Yue Wu, Zhongdao Wang, James
 568 Kwok, Ping Luo, Huchuan Lu, et al. Pixart- α : Fast training of diffusion transformer for photore-
 569 alistic text-to-image synthesis. In *ICLR*, 2024b.

570 Liang Chen, Shuai Bai, Wenhao Chai, Weichu Xie, Haozhe Zhao, Leon Vinci, Junyang Lin, and
 571 Baobao Chang. Multimodal representation alignment for image generation: Text-image inter-
 572 leaved control is easier than you think. *arXiv preprint arXiv:2502.20172*, 2025b.

573 Sixiang Chen, Jinbin Bai, Zhuoran Zhao, Tian Ye, Qingyu Shi, Donghao Zhou, Wenhao Chai, Xin
 574 Lin, Jianzong Wu, Chao Tang, et al. An empirical study of gpt-4o image generation capabilities.
 575 *arXiv preprint arXiv:2504.05979*, 2025c.

576 Xiaokang Chen, Zhiyu Wu, Xingchao Liu, Zizheng Pan, Wen Liu, Zhenda Xie, Xingkai Yu, and
 577 Chong Ruan. Janus-pro: Unified multimodal understanding and generation with data and model
 578 scaling. *arXiv preprint arXiv:2501.17811*, 2025d.

579 Jacob Devlin. Bert: Pre-training of deep bidirectional transformers for language understanding.
 580 *arXiv preprint arXiv:1810.04805*, 2018.

581 Runpei Dong, Chunrui Han, Yuang Peng, Zekun Qi, Zheng Ge, Jinrong Yang, Liang Zhao, Jianjian
 582 Sun, Hongyu Zhou, Haoran Wei, et al. Dreamllm: Synergistic multimodal comprehension and
 583 creation. *arXiv preprint arXiv:2309.11499*, 2023.

584 Patrick Esser, Sumith Kulal, Andreas Blattmann, Rahim Entezari, Jonas Müller, Harry Saini, Yam
 585 Levi, Dominik Lorenz, Axel Sauer, Frederic Boesel, et al. Scaling rectified flow transformers for
 586 high-resolution image synthesis. In *Forty-first International Conference on Machine Learning*,
 587 2024.

594 Lijie Fan, Tianhong Li, Siyang Qin, Yuanzhen Li, Chen Sun, Michael Rubinstein, Deqing Sun,
 595 Kaiming He, and Yonglong Tian. Fluid: Scaling autoregressive text-to-image generative models
 596 with continuous tokens. *arXiv preprint arXiv:2410.13863*, 2024.

597

598 Chaoyou Fu, Peixian Chen, Yunhang Shen, Yulei Qin, Mengdan Zhang, Xu Lin, Jinrui Yang, Xiawu
 599 Zheng, Ke Li, Xing Sun, et al. Mme: A comprehensive evaluation benchmark for multimodal
 600 large language models. *arXiv preprint arXiv:2306.13394*, 2023.

601 Yuying Ge, Sijie Zhao, Jinguo Zhu, Yixiao Ge, Kun Yi, Lin Song, Chen Li, Xiaohan Ding, and Ying
 602 Shan. Seed-x: Multimodal models with unified multi-granularity comprehension and generation.
 603 *arXiv preprint arXiv:2404.14396*, 2024.

604

605 Dhruba Ghosh, Hannaneh Hajishirzi, and Ludwig Schmidt. Geneval: An object-focused frame-
 606 work for evaluating text-to-image alignment. *Advances in Neural Information Processing Systems*
 607 (*NeurIPS*), 36, 2024.

608 Jianyuan Guo, Hanting Chen, Chengcheng Wang, Kai Han, Chang Xu, and Yunhe Wang. Vi-
 609 sion superalignment: Weak-to-strong generalization for vision foundation models. *arXiv preprint*
 610 *arXiv:2402.03749*, 2024.

611

612 Kaiming He, Xinlei Chen, Saining Xie, Yanghao Li, Piotr Dollár, and Ross Girshick. Masked au-
 613 toencoders are scalable vision learners. In *Proceedings of the IEEE/CVF conference on computer*
 614 *vision and pattern recognition (CVPR)*, pp. 16000–16009, 2022.

615 Jonathan Ho, Ajay Jain, and Pieter Abbeel. Denoising diffusion probabilistic models. In *NeurIPS*,
 616 2020.

617

618 Drew A Hudson and Christopher D Manning. Gqa: A new dataset for real-world visual reasoning
 619 and compositional question answering. In *Proceedings of the IEEE/CVF conference on computer*
 620 *vision and pattern recognition*, pp. 6700–6709, 2019.

621

622 Shankar Kantharaj, Rixie Tiffany Leong, Xiang Lin, Ahmed Masry, Megh Thakkar, Enamul Hoque,
 623 and Shafiq Joty. Chart-to-text: A large-scale benchmark for chart summarization. In Smaranda
 624 Muresan, Preslav Nakov, and Aline Villavicencio (eds.), *Proceedings of the 60th Annual Meet-
 625 ing of the Association for Computational Linguistics (Volume 1: Long Papers)*, pp. 4005–4023.
 626 Association for Computational Linguistics, 2022.

627

628 Alexander Kirillov, Eric Mintun, Nikhila Ravi, Hanzi Mao, Chloé Rolland, Laura Gustafson, Tete
 629 Xiao, Spencer Whitehead, Alexander C. Berg, Wan-Yen Lo, Piotr Dollár, and Ross B. Girshick.
 Segment anything. In *ICCV*, 2023.

630

631 Black Forest Labs. Announcing black forest labs, 2024. <https://blackforestlabs.ai/announcing-black-forest-labs/>.

632

633 Tianhong Li, Yonglong Tian, He Li, Mingyang Deng, and Kaiming He. Autoregressive image
 634 generation without vector quantization. *Advances in Neural Information Processing Systems*, 37:
 635 56424–56445, 2024a.

636

637 Zijie Li, Henry Li, Yichun Shi, Amir Barati Farimani, Yuval Kluger, Linjie Yang, and Peng Wang.
 638 Dual diffusion for unified image generation and understanding, 2024b. URL <https://arxiv.org/abs/2501.00289>.

639

640 Zijie Li, Henry Li, Yichun Shi, Amir Barati Farimani, Yuval Kluger, Linjie Yang, and Peng Wang.
 641 Dual diffusion for unified image generation and understanding. *arXiv preprint arXiv:2501.00289*,
 642 2024c.

643

644 Tsung-Yi Lin, Michael Maire, Serge Belongie, James Hays, Pietro Perona, Deva Ramanan, Piotr
 645 Dollár, and C Lawrence Zitnick. Microsoft coco: Common objects in context. In *ECV*, 2014.

646

647 Dongyang Liu, Shitian Zhao, Le Zhuo, Weifeng Lin, Yu Qiao, Hongsheng Li, and Peng Gao.
 648 Lumina-mgpt: Illuminate flexible photorealistic text-to-image generation with multimodal gener-
 649 ative pretraining, 2024a. URL <https://arxiv.org/abs/2408.02657>.

648 Hao Liu, Wilson Yan, Matei Zaharia, and Pieter Abbeel. World model on million-length video and
 649 language with ringattention. *arXiv preprint arXiv:2402.08268*, 2024b.
 650

651 Hao Liu, Wilson Yan, Matei Zaharia, and Pieter Abbeel. World model on million-length video and
 652 language with ringattention. *arXiv preprint*, 2024c.
 653

654 Haotian Liu, Chunyuan Li, Qingyang Wu, and Yong Jae Lee. Visual instruction tuning. *NeurIPS*,
 655 2024d.
 656

657 Yuan Liu, Haodong Duan, Yuanhan Zhang, Bo Li, Songyang Zhang, Wangbo Zhao, Yike Yuan,
 658 Jiaqi Wang, Conghui He, Ziwei Liu, et al. Mmbench: Is your multi-modal model an all-around
 659 player? In *ECCV*, 2024e.
 660

661 Aaron Lou, Chenlin Meng, and Stefano Ermon. Discrete diffusion modeling by estimating the ratios
 662 of the data distribution. *arXiv preprint arXiv:2310.16834*, 2023.
 663

664 Pan Lu, Swaroop Mishra, Tony Xia, Liang Qiu, Kai-Wei Chang, Song-Chun Zhu, Oyvind Tafjord,
 665 Peter Clark, and Ashwin Kalyan. Learn to explain: Multimodal reasoning via thought chains for
 666 science question answering. In *NeurIPS*, 2022.
 667

668 Xinyin Ma, Rupeng Yu, Gongfan Fang, and Xinchao Wang. dkv-cache: The cache for diffusion
 669 language models. *arXiv preprint arXiv:2505.15781*, 2025.
 670

671 Yiyang Ma, Xingchao Liu, Xiaokang Chen, Wen Liu, Chengyue Wu, Zhiyu Wu, Zizheng Pan,
 672 Zhenda Xie, Haowei Zhang, Liang Zhao, et al. Janusflow: Harmonizing autoregression and recti-
 673 fied flow for unified multimodal understanding and generation. *arXiv preprint arXiv:2411.07975*,
 674 2024.
 675

676 Hui Mao, Ming Cheung, and James She. Deepart: Learning joint representations of visual arts.
 677 In *Proceedings of the 25th ACM international conference on Multimedia*, pp. 1183–1191. ACM,
 678 2017.
 679

680 OpenAI. Addendum to gpt-4o system card: 4o image generation, 2025. URL <https://openai.com/index/gpt-4o-image-generation-system-card-addendum/>. Accessed:
 681 2025-04-02.
 682

683 Junting Pan, Keqiang Sun, Yuying Ge, Hao Li, Haodong Duan, Xiaoshi Wu, Renrui Zhang, Aojun
 684 Zhou, Zipeng Qin, Yi Wang, Jifeng Dai, Yu Qiao, and Hongsheng Li. Journeydb: A benchmark
 685 for generative image understanding, 2023.
 686

687 Xichen Pan, Satya Narayan Shukla, Aashu Singh, Zhuokai Zhao, Shlok Kumar Mishra, Jialiang
 688 Wang, Zhiyang Xu, Juhai Chen, Kunpeng Li, Felix Juefei-Xu, et al. Transfer between modalities
 689 with metaqueries. *arXiv preprint arXiv:2504.06256*, 2025.
 690

691 Dustin Podell, Zion English, Kyle Lacey, Andreas Blattmann, Tim Dockhorn, Jonas Müller, Joe
 692 Penna, and Robin Rombach. Sdxl: Improving latent diffusion models for high-resolution image
 693 synthesis. *arXiv preprint arXiv:2307.01952*, 2023.
 694

695 Alec Radford, Jong Wook Kim, Chris Hallacy, Aditya Ramesh, Gabriel Goh, Sandhini Agar-
 696 wal, Girish Sastry, Amanda Askell, Pamela Mishkin, Jack Clark, Gretchen Krueger, and Ilya
 697 Sutskever. Learning transferable visual models from natural language supervision. In *ICML*,
 698 2021.
 699

700 Aditya Ramesh, Prafulla Dhariwal, Alex Nichol, Casey Chu, and Mark Chen. Hierarchical text-
 701 conditional image generation with clip latents. *arXiv preprint arXiv:2204.06125*, 2022.
 702

703 Robin Rombach, Andreas Blattmann, Dominik Lorenz, Patrick Esser, and Björn Ommer. High-
 704 resolution image synthesis with latent diffusion models. In *CVPR*, 2022.
 705

706 Christoph Schuhmann, Richard Vencu Beaumont, Romain Gordon Vencu, Clayton Coombes, Arun
 707 Katta, Robin Kaczmarczyk, and Jenia Jitsev. Laion-5b: An open large-scale dataset for training
 708 next-generation image-text models. <https://laion.ai/blog/laion-5b/>, 2022. Ac-
 709 cessed: 2025-09-25.
 710

702 Quan Sun, Qiying Yu, Yufeng Cui, Fan Zhang, Xiaosong Zhang, Yueze Wang, Hongcheng Gao,
 703 Jingjing Liu, Tiejun Huang, and Xinlong Wang. Generative pretraining in multimodality. *arXiv*
 704 *preprint arXiv:2307.05222*, 2023.

705 Alexander Swerdlow, Mihir Prabhudesai, Siddharth Gandhi, Deepak Pathak, and Katerina Fragki-
 706 adaki. Unified multimodal discrete diffusion. *arXiv preprint arXiv:2503.20853*, 2025a.

707 Alexander Swerdlow, Mihir Prabhudesai, Siddharth Gandhi, Deepak Pathak, and Katerina Fragki-
 708 adaki. Unified multimodal discrete diffusion. *arXiv preprint arXiv:2503.20853*, 2025b. doi:
 709 10.48550/arXiv.2503.20853.

710 Chameleon Team. Chameleon: Mixed-modal early-fusion foundation models. *arXiv preprint*
 711 *arXiv:2405.09818*, 2024.

712 Shengbang Tong, David Fan, Jiachen Zhu, Yunyang Xiong, Xinlei Chen, Koustuv Sinha, Michael
 713 Rabbat, Yann LeCun, Saining Xie, and Zhuang Liu. Metamorph: Multimodal understanding and
 714 generation via instruction tuning. *arXiv preprint arXiv:2412.14164*, 2024.

715 Hugo Touvron, Thibaut Lavril, Gautier Izacard, Xavier Martinet, Marie-Anne Lachaux, Timothée
 716 Lacroix, Baptiste Rozière, Naman Goyal, Eric Hambro, Faisal Azhar, et al. Llama: Open and
 717 efficient foundation language models. *arXiv preprint arXiv:2302.13971*, 2023.

718 Chunwei Wang, Guansong Lu, Junwei Yang, Runhui Huang, Jianhua Han, Lu Hou, Wei Zhang,
 719 and Hang Xu. Illume: Illuminating your llms to see, draw, and self-enhance. *arXiv preprint*
 720 *arXiv:2412.06673*, 2024a.

721 Xinlong Wang, Xiaosong Zhang, Zhengxiong Luo, Quan Sun, Yufeng Cui, Jinsheng Wang, Fan
 722 Zhang, Yueze Wang, Zhen Li, Qiying Yu, et al. Emu3: Next-token prediction is all you need.
 723 *arXiv preprint arXiv:2409.18869*, 2024b.

724 Yecheng Wu, Zhuoyang Zhang, Junyu Chen, Haotian Tang, Dacheng Li, Yunhao Fang, Ligeng
 725 Zhu, Enze Xie, Hongxu Yin, Li Yi, et al. Vila-u: a unified foundation model integrating visual
 726 understanding and generation. *arXiv preprint arXiv:2409.04429*, 2024.

727 Jinheng Xie, Weijia Mao, Zechen Bai, David Junhao Zhang, Weihao Wang, Kevin Qinghong Lin,
 728 Yuchao Gu, Zhijie Chen, Zhenheng Yang, and Mike Zheng Shou. Show-o: One single transformer
 729 to unify multimodal understanding and generation. *arXiv preprint arXiv:2408.12528*, 2024.

730 Yi Xin, Qi Qin, Siqi Luo, Kaiwen Zhu, Juncheng Yan, Yan Tai, Jiayi Lei, Yuewen Cao, Keqi Wang,
 731 Yibin Wang, et al. Lumina-dimoo: An omni diffusion large language model for multi-modal
 732 generation and understanding. *arXiv preprint arXiv:2510.06308*, 2025.

733 Ling Yang, Ye Tian, Bowen Li, Xinchen Zhang, Ke Shen, Yunhai Tong, and Mengdi Wang. Mmada:
 734 Multimodal large diffusion language models. *arXiv preprint arXiv:2505.15809*, 2025a.

735 Ling Yang, Ye Tian, Bowen Li, Xinchen Zhang, Ke Shen, Yunhai Tong, and Mengdi Wang. Mmada:
 736 Multimodal large diffusion language models. *arXiv preprint arXiv:2505.15809*, 2025b.

737 Xiang Yue, Yuansheng Ni, Kai Zhang, Tianyu Zheng, Ruoqi Liu, Ge Zhang, Samuel Stevens,
 738 Dongfu Jiang, Weiming Ren, Yuxuan Sun, Cong Wei, Bota Yu, Ruibin Yuan, Renliang Sun,
 739 Ming Yin, Boyuan Zheng, Zhenzhu Yang, Yibo Liu, Wenhao Huang, Huan Sun, Yu Su, and
 740 Wenhui Chen. Mmmu: A massive multi-discipline multimodal understanding and reasoning
 741 benchmark for expert agi. In *CVPR*, 2024.

742 Chuyang Zhao, Yuxing Song, Wenhao Wang, Haocheng Feng, Errui Ding, Yifan Sun, Xinyan Xiao,
 743 and Jingdong Wang. Monoformer: One transformer for both diffusion and autoregression. *arXiv*
 744 *preprint arXiv:2409.16280*, 2024.

745 Mengyu Zheng, Yehui Tang, Zhiwei Hao, Kai Han, Yunhe Wang, and Chang Xu. Adapt without for-
 746 getting: Distill proximity from dual teachers in vision-language models. In *European Conference*
 747 *on Computer Vision*, pp. 109–125. Springer, 2024.

748 Chunting Zhou, Lili Yu, Arun Babu, Kushal Tirumala, Michihiro Yasunaga, Leonid Shamis, Jacob
 749 Kahn, Xuezhe Ma, Luke Zettlemoyer, and Omer Levy. Transfusion: Predict the next token and
 750 diffuse images with one multi-modal model. *arXiv preprint arXiv:2408.11039*, 2024.

756 APPENDIX
757758 APPENDIX OVERVIEW
759760 This appendix provides additional discussions, results, and analyses to complement the main paper.
761 It is organized as follows:
762

- 763 • **Related Work** (Sec. A): We review unified multimodal models for understanding and gen-
764 eration, with a focus on autoregressive and diffusion-based paradigms, as well as recent
765 advances in masked image modeling.
- 766 • **Additional Qualitative Results** (Sec. B): We present extended visualizations for several
767 tasks, including image captioning, text-to-image generation, visual question answering,
768 and image-guided text editing.
- 769 • **Additional Experimental Results** (Sec. C): We present more experimental results.
- 770 • **Additional Ablation Studies** (Sec. D): We present extended ablation studies.
- 771 • **Inference Time Analysis** (Sec. E): We analyze inference efficiency by comparing autore-
772 gressive decoding with discrete diffusion, providing FLOPs complexity and speed bench-
773 marks.
- 774 • **Generated Results Step by Step** (Sec. F): We illustrate the reverse discrete diffusion pro-
775 cess in detail, showing intermediate decoding steps and examples of progressive generation.
- 776 • **Discussion** (Sec. G): We reflect on the limitations of our approach and its broader impacts,
777 including potential applications and risks of misuse.
- 778 • **Use of Large Language Models**: We clarify the role of large language models during
779 paper preparation, emphasizing that they were only used for minor editing and polishing.

781 A RELATED WORK
782783 A.1 UNIFIED MODELS FOR GENERATION AND UNDERSTANDING
784785 The success of LLMs in language modeling has inspired efforts to extend unified generation to mul-
786 timodal domains. However, the divergence between autoregressive and diffusion-based paradigms
787 presents fundamental architectural trade-offs. Autoregressive models naturally handle language, and
788 several works (Sun et al., 2023; Wang et al., 2024a; Tong et al., 2024; Ge et al., 2024; Dong et al.,
789 2023; Chen et al., 2025b) extend this by connecting vision modules to LLMs via adapters or instruc-
790 tion tuning, with LLMs serving as planning modules that produce intermediate representations for
791 image generation. While effective to some extent, these paradigms often exhibit limited interaction
792 between text and image modalities and struggle with content consistency, particularly in image-
793 to-image generation and complex instruction-based synthesis. To address these limitations, recent
794 research explores unified generation models that integrate understanding and generation within a
795 single architecture. We categorize these into four major paradigms (see Fig. 6):796 **Fully Autoregressive**: Both text and image are tokenized into discrete sequences and modeled with
797 an AR Transformer (Liu et al., 2024b; Team, 2024; Wu et al., 2024; Wang et al., 2024b; Chen
798 et al., 2025d; Liu et al., 2024a; Guo et al., 2024; Zheng et al., 2024). These models achieve strong
799 cross-modal generation but suffer from high latency due to sequential decoding.800 **Text AR, Image Diffusion**: LLMs generate text tokens while image synthesis is delegated to pre-
801 trained continuous diffusion backbones (Zhou et al., 2024; Zhao et al., 2024; Ma et al., 2024) or
802 discrete diffusion (Xie et al., 2024). Though visually strong, these models are not truly unified, as
803 they rely on separate architectures and token spaces.804 **Image Diffusion, Text Discrete Diffusion**: Emerging models experiment with discrete diffusion for
805 text and images (Li et al., 2024c), though many, like Dual-Diffusion, still use continuous diffusion
806 for image synthesis, failing to realize true modality symmetry.807 **Fully Discrete Diffusion**: Recent work like UniDisc (Swerdlow et al., 2025a) pioneers full-token
808 discrete diffusion over shared Transformer backbones. These models support parallel sampling and
809 native integration, but currently lag behind in generation fidelity and scale.

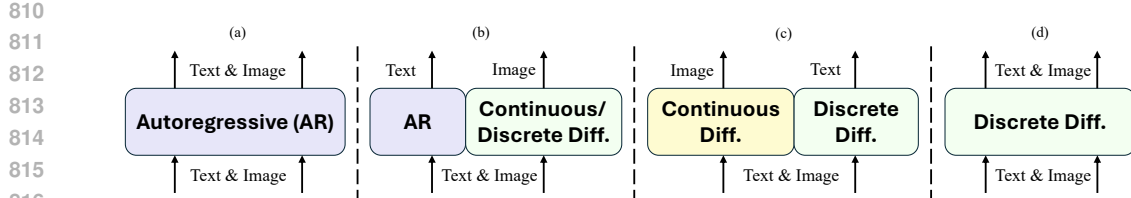


Figure 6: Four types of unified generative models. More details can be found in Sec. A.

Among these, the GPT-4o (OpenAI, 2025) model represents a significant advance as a unified multimodal generative system. However, its closed-source nature obscures critical architectural and training details, and its success may be largely attributable to scale rather than architectural novelty (Chen et al., 2025c).

A.2 MASKED IMAGE MODELING

Masked Image Modeling (MIM) has emerged as a powerful self-supervised learning paradigm in computer vision, drawing inspiration from the success of Masked Language Modeling (MLM) in NLP, notably BERT (Devlin, 2018). The fundamental principle of MIM involves obscuring portions of an image, which could be raw pixels (MAE (He et al., 2022)), latent patches of pixels, or even discrete latent tokens (BEiT (Bao et al., 2021), MaskGIT (Chang et al., 2022)), and training a model, typically an autoencoder, to predict or reconstruct this missing information by leveraging the context provided by the visible parts.

MaskGIT (Chang et al., 2022) introduced parallel decoding via iterative token refinement, inspiring discrete diffusion models. Recent work such as RandomAR (Fan et al., 2024) and MAR (Li et al., 2024a) formalize this as random-order or masked autoregressive generation, blending AR and MIM principles. The major conceptual difference between RandomAR/MAR and MaskGIT is in the scanning order at inference time.

This class of techniques forms the conceptual foundation of discrete diffusion over tokenized spaces and plays a critical role in modern unified models. We will introduce discrete diffusion in the next section.

A.3 RELATIONSHIP TO CONCURRENT WORK

Our main contribution is to show that a unified, *visual-prior* fully discrete diffusion model can be both effective and data-efficient on image understanding tasks, rather than only on text-to-image generation tasks. Regarding the distinction from discrete diffusion works (Swerdlow et al., 2025b; Yang et al., 2025a; Xin et al., 2025) we think that unified models should allow for multiple design choices. Our goal is to demonstrate that a visual-first, fully discrete diffusion backbone can be a practical and competitive alternative to the more common “LLM-first” unified paradigm, and we believe this is a fundamental design choice.

Concretely, prior unified discrete diffusion models such as UniDisc (Swerdlow et al., 2025b) are trained from scratch on multimodal data and therefore lack strong visual priors. As a result, they significantly underperform early diffusion baselines such as Stable Diffusion 1.5 (Rombach et al., 2022) and do not support vision-language reasoning tasks like VQA (Antol et al., 2015). In contrast, Mudit is the first unified discrete diffusion model built on top of a pretrained high-resolution text-to-image backbone (Meissonic), with a lightweight text decoder on top. This visual prior is not an implementation detail: it improves the scalability and generalization behavior of discrete diffusion through a text well-aligned visual backbone.

B ADDITIONAL QUALITATIVE RESULTS

Image-to-text Generation. We present more examples for image-to-text generation in Fig. 7.

Text-to-image Generation. We present more examples for text-to-image generation in Fig. 8.

864 **Visual Question Answering.** We present more examples for visual question answering in Fig. 9.
 865 Mudit reliably identifies fine-grained attributes (e.g., “blonde” hair), object categories (e.g., “bea-
 866 gle”), and physical affordances (e.g., answering “No” to crossing at a red light). Notably, it also
 867 handles commonsense reasoning and spatial localization, such as inferring traffic legality or locat-
 868 ing vehicles on the street.

869 **Image-guided text editing.** Zero-shot text-guided image editing performance is already verified
 870 and presented in Meissonic (Bai et al., 2025). As the successor to Meissonic, we present Mudit’s
 871 performance on the image-guided text editing task, where the model completes a masked sentence
 872 based on the input image. As shown in Fig. 10, given a partially masked caption and an image,
 873 Mudit fills in the blanks with semantically and visually grounded phrases.

875 C ADDITIONAL EXPERIMENTAL RESULTS

877 We provide a detailed breakdown of the MME benchmark results in the Tab. 8. Mudit demon-
 878 strates strong performance in existence, color, and scene understanding, while also exhibiting solid
 879 reasoning capabilities.

881 Table 8: Detailed MME results.

883 Category	884 Task	885 Score
886 Perception	887 Existence	888 135.00
	889 Count	890 78.33
	891 Position	892 53.33
	893 Color	894 140.00
	895 Posters	896 62.24
	897 Celebrity	898 56.18
	899 Scene	900 107.25
	901 Landmark	902 94.50
	903 Artwork	904 76.00
905 Cognition	906 OCR	907 52.50
	908 Total	909 855.34
	910 Commonsense Reasoning	911 78.57
	912 Numerical Calculation	913 90.00
914 Text Translation	915 Code Reasoning	916 57.89
	917 Total	918 283.97

902 D ADDITIONAL ABLATION STUDIES

904 D.1 ABLATION STUDY ON THE CFG FOR IMAGE-TO-TEXT GENERATION

906 As shown in Tab. 9. We report performance on MS-COCO captioning and VQAv2 benchmarks.
 907 Moderate CFG values (e.g., 1.5) yield the best results, while higher scales lead to degraded per-
 908 formance.

910 E INFERENCE TIME ANALYSIS

912 As shown in Fig. 13, autoregressive multimodal models are inherently limited by token-by-token
 913 decoding, which constrains their inference speed. Mudit overcomes this bottleneck with a parallel
 914 discrete diffusion decoder, reducing average latency to just 1.49 seconds, achieving a 4× to 11×
 915 speedup over competitive baselines (4.2× faster than Qwen-2.5-VL, 5.6× than Show-o, 8.1× than
 916 BLIP-2, and 10.9× than LLaVA-1.6).

917 Besides, we present detailed FLOPs comparison between Autoregressive and Discrete Diffusion.

918 Table 9: Ablation study on the effect of classifier-free guidance (CFG) scale.
919

Dataset	CFG = 1	CFG = 1.5	CFG = 2	CFG = 2.5	CFG = 3
MS-COCO	57.2	59.9	58.2	51.3	47.2
VQAv2	65.8	68.2	64.7	55.4	49.2

920
921 Table 10: Comparison of model efficiency across different resolutions and steps. We report through-
922 put for both text-to-image generation (images per second) and image-to-text tasks (tokens per sec-
923 ond). Mudit achieves the best overall balance, matching the highest text-to-image throughput while
924 significantly outperforming others in image-to-text speed.
925

Model	Image Res	Steps	Text-to-Image (img/s)	Image-to-Text (token/s)
Meissonic	1024	32	0.23	–
UniDisc	512	32	0.89	79.36
Monetico	512	32	1.00	–
D-DiT	512	28	0.62	26.89
Mudit	512	32	1.00	99.98

926
927 **Autoregressive (AR) without KV Cache:**
928929
930

- At step t , the model attends over t previous tokens.
- Per-step attention FLOPs: $O(t^2D)$.
- Total FLOPs:

931
932
933
934
$$\sum_{t=1}^L O(t^2D) = O\left(D \sum_{t=1}^L t^2\right) = O\left(D \cdot \frac{L(L+1)(2L+1)}{6}\right) = O(L^3D)$$

935
936 **Autoregressive (AR) with KV Cache:**
937938

- At step t , Q is computed for 1 token, and attends to t K/V keys.
- Per-step attention FLOPs: $O(tD)$.
- Total FLOPs:

939
940
941
$$\sum_{t=1}^L O(tD) = O\left(D \sum_{t=1}^L t\right) = O\left(D \cdot \frac{L(L+1)}{2}\right) = O(L^2D)$$

942
943 **Discrete Diffusion:**
944945

- Each step updates the full sequence (length L) in parallel.
- Per-step attention FLOPs: $O(L^2D)$.
- Total FLOPs:

946
$$T \cdot O(L^2D) = O(TL^2D), \quad T \ll L$$

947
948 While discrete diffusion may appear less efficient than autoregressive (AR) models with KV caching
949 in terms of theoretical FLOPs, it offers a significant advantage over AR without caching—achieving
950 an L/T speedup by updating the full token sequence in parallel over T iterations. In practice, the
951 higher degree of parallelism leads to competitive, and often faster, inference speed compared to
952 AR models, especially when considering real-world GPU throughput. As KV cache techniques for
953 discrete diffusion are rapidly evolving (Ma et al., 2025), we expect further acceleration in the near
954 future, narrowing the theoretical speed gap even with KV-cache AR baselines.
955956
957 In Tab. 10, we compared Mudit against other non-autoregressive models, running all tests on a
958 single A800 80 GB GPU. Mudit demonstrated a clear advantage in both image and text generation.
959

972 F GENERATED RESULTS STEP BY STEP
973

974 Muddit frames text generation as reverse discrete diffusion over a fixed-length sequence of 77 token
975 indices. At inference time, the model performs $16 \leq T \leq 32$ denoising steps, starting from a max-
976 imally entropic prior where every token is masked. At each step t , a parameter-shared transformer
977 G predicts a categorical distribution over all positions in parallel, and a sampler S selects the next
978 sequence:

$$979 \mathbf{x}_{t-1} = S(G(\mathbf{x}_t, \mathbf{c}, t), \mathbf{x}_t, t), \quad t = T, \dots, 1, \quad (12)$$

980 where $\mathbf{x}_t \in \mathbb{V}^{77}$ is the token sequence at step t , and \mathbf{c} denotes conditioning inputs. The logits can be
981 tempered or top- k filtered before sampling each token independently. The resulting sequence \mathbf{x}_{t-1}
982 seeds the next step, enabling fast, parallel decoding without autoregressive constraints.

983 Because all positions are updated in parallel, Muddit preserves global syntactic and semantic struc-
984 ture throughout the reverse diffusion process—unlike left-to-right autoregressive models, which can
985 only condition on past predictions. Empirically, as few as $16 \leq T \leq 32$ steps are sufficient to
986 approximate the natural language distribution with high fidelity. Thus, Muddit unifies diffusion gen-
987 eration with parallel decoding, effectively overcoming the serial bottleneck that limits conventional
988 autoregressive multimodal models.

989 We present 2 examples in Fig. 11 and Fig. 12.

991 G DISCUSSION
992993 G.1 LIMITATIONS
994

995 While Muddit advances discrete diffusion for unified multimodal generation, it still presents several
996 limitations. First, due to its token-level discrete representation, the model may underperform con-
997 tinuous diffusion models in generating photorealistic or high-resolution images. Second, Muddit is
998 initialized from a pretrained text-to-image foundation model, which offers strong visual priors but
999 limits its capacity for rich text understanding and generation compared to the latest large language
1000 models. This makes it less suitable for tasks that require long-form understanding and generation or
1001 deep linguistic reasoning.

1003 G.2 BROADER IMPACTS
1004

1005 Muddit explores a new paradigm in multimodal generation by leveraging a strong visual prior as
1006 the backbone, in contrast to the prevailing trend of scaling large language models. This offers a
1007 complementary path toward efficient, grounded multimodal generation, particularly in vision-centric
1008 applications. The model’s ability to generate aligned visual and textual outputs in a fast, parallel
1009 manner could benefit downstream tasks, especially in completion-based scenarios such as masked
1010 captioning, image editing, and code implementation. However, as with all generative models, there
1011 remains a risk of misuse in synthetic content creation.

1012 H THE USE OF LARGE LANGUAGE MODELS
1013

1014 During the preparation of this paper, large language models were used only for language polishing
1015 and minor editing. All research ideas, methods, and experimental results were carried out entirely
1016 by the human authors.

1018
1019
1020
1021
1022
1023
1024
1025

1026

1027

1028

1029

1030

1031

1032

1033

1034

1035

1036

1037

1038

1039

1040

1041

1042

1043

1044

1045

1046

1047

1048

1049

1050

1051

1052

1053

1054

1055

1056

1057

1058

1059

1060

1061

1062

1063

1064

1065

1066

1067

1068

1069

1070

1071

1072

1073

1074

1075

1076

1077

1078

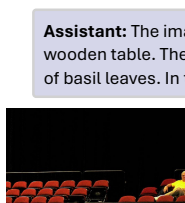
1079



Assistant: The image depicts a charming street scene with a cobblestone pavement and tall buildings. A white dog is resting. The dog is lying down near the bicycle on the street. To the left of the street, there is an old bicycle parked to the side of the street.



Assistant: The image is a black - and - white photograph featuring three individuals sitting together on a bench. They appear to be in an urban setting, as indicated by the trees and buildings in the background. The individuals are dressed in police uniforms, with one person looking behind the first individual from the second individual.



Assistant: The image depicts an elderly man standing on a city street, wearing a red jacket and a black cap talking on cell phone to his ear. The background shows a crowd of people walking around, some of whom are handbags and others visible in the distance. The crowd appears to be the middle of a busy area.



Assistant: The image depicts a close - up of a large, round pizza placed on a wooden table. The pizza is topped with cheese, and there are several pieces of basil leaves. In the background, there are other people sitting around.



Assistant: The image depicts a tennis match on a blue court. The tennis match is set against a backdrop of a blue court. The player, wearing a white shirt and white shorts, is in mid action and holding a tennis racket, possibly preparing for a shot. The court has a row of seats.



Assistant: The image depicts a vibrant and colorful arrangement of umbrellas hanging from the branches of trees. The umbrellas come in color and shape, including pink, red, and yellow, blue, and purple. They are arranged in a circular pattern across the umbrellas, creating a visually appealing display. The background features a mix of green trees and foliage, suggesting an outdoor.



Assistant: The image depicts a bustling urban street scene with several notable elements. In the foreground, there is a tall green clock tower with a clock face and a pole, which stands prominently on the street. The clock has a clock face on it, indicating the time. In the background, there are several parked cars.



Assistant: The image depicts a person surfing on a surfboard on a large wave. The surfer is in mid-air, with his arms bent, navigating the balance of the wave. The background shows a clear blue sky, adding depth to the overall scene. The surfer seems to be in the middle of the the wave.



Assistant: The image depicts a giraffe standing on a grassy field in a rural outdoor setting. The background features a clear blue sky with some scattered clouds, and there are trees in the distant distance. The giraffe appears to be looking towards a distant horizon.



Assistant: The image depicts a stop sign in front of a grassy field with majestic mountains in the background. The sky is clear with a scattered clouds, and snow-capped mountains rise in the background. The scene appears to be in a rural setting.



Figure 7: Image-to-text generated results.

1080

1081

1082

1083

1084

1085

1086

1087

1088

Human: An editorial fashion photo portrait of a striking avant-garde model with bubble details. Iridescent art and pop surrealism influence the image's ethereal feel. Pastel aesthetic hues of soft pink, tangerine, and green create a dreamy backdrop. Seamless pink background, studio lighting emphasizes the model's silhouette against the soft pastel palette.

1092

1093

1094

1095

1096

1097

1098

1099

1100

1101

1102

1103

Human: A quaint small town nestled amidst snow-capped hills, bathed in the soft, golden hues of dusk. The sky is a tapestry of twilight blue and orange, casting long shadows across cobblestone streets as frosted trees stand bare against the fading light. A sense of quiet peace emanates from the scene.



1104

1105

1106

1107

1108

1109



1110

1111

1112

1113

1114

1115

1116

1117

1118

1119

1120

1121

1122

1123

1124

1125

1126

1127

1128

1129

1130

1131

1132

1133

Human: A vibrant Japanese garden, inspired by Van Gogh's swirling brushstrokes. Vivid reds, yellows, blues, and greens dominate the scene. Cherry blossoms bloom in full splendor against a backdrop of ancient stone lanterns, rendered with lush foliage and dappled sunlight. The effect is heightened by 4K resolution and cinematic depth.



Figure 8: Text-to-image generation results.

1134

1135

1136

1137

1138

1139

1140

1141

1142

1143

1144

1145

1146

1147

1148

1149

1150

1151

1152

1153

1154

1155

1156

1157

1158

1159

1160

1161

1162

1163

1164

1165

1166

1167



Human: What color is the kid's hair?

Assistant: The color of the kid's hair is blonde.



Human: Can someone legally walk across the street right now?

Assistant: No.



Human: What brand of dogs are these?

Assistant: The brand of dogs are beagle.



Human: What is flying in the picture?

Assistant: Kite.



Human: What eating utensil is pictured?

Assistant: Fork.



Human: Where are the cars?

Assistant: The cars are on the street.

Figure 9: Visual question answering results.



<mask> <mask> <mask> lying on a grassy surface. <mask> <mask> has a <mask> fur with darker patches on its face and ears, looking directly at <mask> <mask>. the bear's mouth is slightly <mask>, revealing its teeth and tongue. the background shows some green grass.

Muddit

Image-guided text editing

A curly bear lying on a grassy surface. the bear has a brown fur with darker patches on its face and ears, looking directly at the camera. the bear's mouth is slightly open, revealing its teeth and tongue. the background shows some green grass.

Figure 10: Image-guided text editing results.

1188
1189
1190
1191
1192
1193
1194
1195
1196
1197
1198



User: Please describe this image.

Figure 11: Image-to-text generated results in each step.

1242
1243
1244
1245
1246
1247
1248
1249
1250
1251



User: Please describe this image.

Figure 12: Image-to-text generated results in each step.

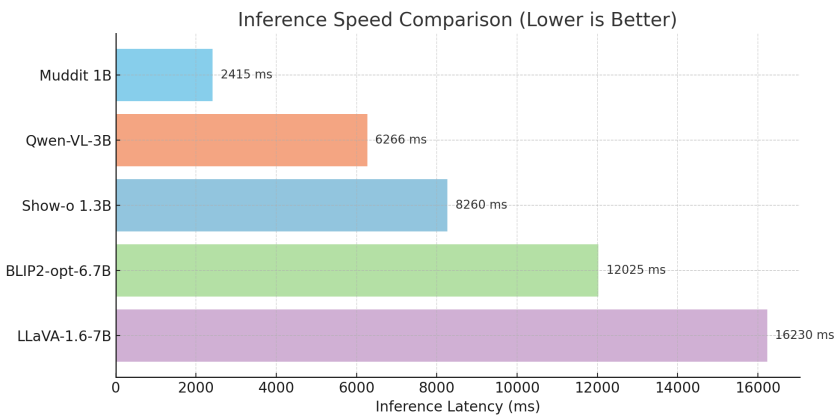


Figure 13: Inference speed comparison. We use 32 inference steps for Muddit and fix the sequence length to 77 across all models.